

# Failure-recovery model with competition between failures in complex networks: a dynamical approach

L. D. Valdez,<sup>1</sup> M. A. Di Muro,<sup>1</sup> and L. A. Braunstein<sup>1,2</sup>

<sup>1</sup>*Instituto de Investigaciones Físicas de Mar del Plata (IFIMAR)-Departamento de Física, Facultad de Ciencias Exactas y Naturales, Universidad Nacional de Mar del Plata-CONICET, Funes 3350, (7600) Mar del Plata, Argentina.*

<sup>2</sup>*Center for Polymer Studies, Boston University, Boston, Massachusetts 02215, USA*

## Abstract

Real systems are usually composed by units or nodes whose activity can be interrupted and restored intermittently due to complex interactions not only with the environment, but also with the same system. Majdandžić *et al.* [Nature Physics **10**, 34 (2014)] proposed a model to study systems in which active nodes fail and recover spontaneously in a complex network and found that in the steady state the density of active nodes can exhibit an abrupt transition and hysteresis depending on the values of the parameters. Here we investigate a model of recovery-failure from a dynamical point of view. Using an effective degree approach we find that the systems can exhibit a temporal sharp decrease in the fraction of active nodes. Moreover we show that, depending on the values of the parameters, the fraction of active nodes has an oscillatory regime which we explain as a competition between different failure processes. We also find that in the non-oscillatory regime, the critical fraction of active nodes presents a discontinuous drop which can be related to a “targeted” k-core percolation process. Finally, using mean field equations we analyze the space of parameters at which hysteresis and oscillatory regimes can be found.

Keywords: Random graphs, networks; Nonlinear dynamics; Percolation

## I. INTRODUCTION

In nature and social networks, node aging effects and external forces introduce perturbations on these systems which affect their functions or even can trigger catastrophic cascade of failures. However many of these systems are able to develop different mechanisms to recover their functionality. For instance, it was recently shown that rat brains under anesthesia pass through discrete metastable states of activity which allows to recover from a state of induced comma to a full consciousness state in a physiological time [1]. In protein network regulation when, for example the DNA is damaged, a specific protein is activated [2]. This produces the arrest of the cell division cycle which prevents the proliferation of cells containing damaged DNA (tumor formation). Then, a biochemical processes involved in DNA repair is initiated. Once this task is completed successfully, the cell resumes its progression so that cell division can take place. If repairing is not possible due to excessive damage, the specific protein leads to apoptosis, *i.e.* programmed cell death.

Recently Majdandžić *et al.* [3] proposed a model to study systems in which nodes fail and recover spontaneously in a complex network. In their model, a node can be in one of the following two states: active or inactive. In particular, nodes can be inactive due to: i) internal failure (independently of the states of their neighbors) or ii) external failure when a fraction of their neighbors are inactive, *i.e.* there is an interaction between nodes and their neighbors. They studied numerically and theoretically, in a mean field approach, the steady state of the process and found that the density of active nodes  $A$  can exhibits an abrupt transition and hysteresis, which mimics the behavior observed in different biological and economical systems [3].

The model proposed by Majdandžić *et al.* [3] can be related to an epidemic model, since active nodes are equivalent to susceptible nodes, *i.e.*, non-infected individuals; and inactive nodes are equivalent to infected ones. As a consequence, the same tools implemented in the field of epidemiology can be extended to models where nodes recover and fail spontaneously as in Ref. [3].

In this manuscript we propose a dynamical model of activation and spontaneous recovery and use the framework from the epidemiology field to describe the dynamics of the process. The study of dynamical processes in complex systems is a very important

area of research since it allows understanding the role of the nonlinearities involved in the processes. There are different theoretical approaches to study the evolution of a disease spreading. One of the most detailed framework is the Markovian equations applied to complex networks, to study the evolution of the spread of an epidemic [4]. In this approach, it is necessary to use an order of  $N$  differential equations, where  $N$  is the size of the network. Another theoretical tool is the effective degree approach, [5] in which the compartments are disaggregated by the states of the nodes of a network (infected or non-infected), and by the number of its neighbors in each state. In particular, in epidemic models such as the Susceptible-Infected-Recovered (SIR) and the Susceptible-Infected-Susceptible (SIS) —see Ref. [5]— the number of equations used to describe the evolution of the density of individuals in different compartments is of the order  $O(k_{\max}^3)$  and  $O(k_{\max}^2)$  respectively, where  $k_{\max}$  is the maximum degree that a node can have. In Ref. [5] it was shown that this approach gives a good agreement between theory and simulations for the SIR and SIS models. Finally, one of the simplest tools to study epidemic process are the equations based on the law of mass action, or simply, mean field (MF) equations [6] which have very little or no information about the topology of the network and disregard any correlation between the states of the nodes. Although sometimes, there is not a good agreement between the theoretical results and the simulations on complex networks, this approach: i) gives a qualitatively description of the process, ii) allows to find analytically the behavior of relevant magnitudes, iii) allows to study the stability of the fixed points in MF easily. For interested readers a more detailed description of the tools applied on epidemic models can be found in [7–11] and references therein.

In this work we apply the degree based framework, used in epidemic processes that spread in complex networks, to describe the evolution of the states on complex networks where active nodes overcome internal, external failures and recovery. In our failure-recovery model active nodes can fail by random internal failures at a rate  $p$  and recover from this kind of failure at a rate  $\gamma_I$ . Active nodes can also fail at a rate  $r$  due to lack of support of their neighborhood and recover at a rate  $\gamma_E$ . Unlike the model presented in Ref [3], here we distinguish between inactive nodes failed by internal and external failures that dynamically compete to “capture” active nodes. Our model mimics some biological systems such as neural networks, where some nodes can exhibit inhibitory or excitatory functions [12].

We find that depending on the values of the parameters, the system exhibits regimes with hysteresis and oscillations. We discuss the relation between our model in the steady state and k-core percolation. Finally, using a MF approach we study the phase diagram of the fraction of active nodes as a function of the parameters, and we show that only for  $\gamma_I < \gamma_E$  the system is able to sustain oscillations.

This paper is organized as following: in Sec. II we present our model and the evolution equations based on the effective degree approach. In Sec. III A we show our dynamical results and in Sec. III B we present the results in the steady state. In Sec. IV we study the stability of the solutions and construct the Lyapunov function in the mean field approach. In Sec. V we present our conclusions.

## II. MODEL

In our failure-recovery model, a node can be in one of the following three compartment states:

- Active ( $\mathcal{A}$ ): nodes which are not failed or damaged,
- Inactive due to internal failure ( $\mathcal{I}$ ):  $\mathcal{A}$  nodes that fail at a rate  $p$  independently of the states of their neighbors. These nodes recover (*i.e* become active) at a rate  $\gamma_I$ ,
- Inactive due to external failure ( $\mathcal{E}$ ):  $\mathcal{A}$  nodes having  $m$  or less active neighbors which fail at a rate  $r$  due to lack of support from their neighbors. These nodes recover at a rate  $\gamma_E$ .

In Fig. 1 we show a schematic of the rules of our spontaneous recovery model.

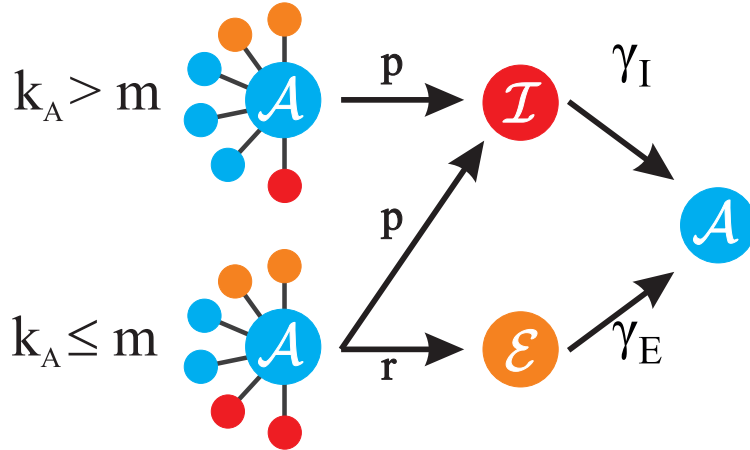


FIG. 1: Schematic representation of the model. Light blue, red and orange nodes represent the active ( $\mathcal{A}$ ), inactive due to internal failure ( $\mathcal{I}$ ) and inactive due to external failure ( $\mathcal{E}$ ), respectively. Active nodes can fail internally with rate  $p$  independently of the number of active neighbors ( $k_A$ ). Active nodes with  $k_A \leq m$  can also fail externally with rate  $r$  due to the lack of support of their neighbors. In the schematic we use  $m = 2$ . The  $\mathcal{E}$  nodes become active at rate  $\gamma_E$  and the  $\mathcal{I}$  ones at rate  $\gamma_I$ .

The particular case of  $\gamma_I = \gamma_E = p = 0$  is the special case of a  $k$ -core percolation process [13–16] in which nodes go through an irreversible transition from state  $\mathcal{A}$  to  $\mathcal{E}$ . In the “random”  $k$ -core percolation, after randomly removing a fraction  $1 - q$  of nodes, a cascade is triggered and all the nodes having  $m$  or less non-removed or living neighbors, are removed. In the steady state, there is a giant component (GC) composed by nodes with more than  $m$  living neighbors, which we call a “compact” sub-graph. It was shown that the final number of living nodes in this process can exhibit a first order phase transition at a critical initial failure  $1 - q_c$  where  $q_c$ , is the initial critical fraction of living nodes in the cascade. In Appendix B 1 we show the equations for the steady state of the “random”  $k$ -core percolation. We will also discuss later the relation between our model and  $k$ -core percolation.

The main theoretical approach that we use in this manuscript to describe our model is the effective degree approach [5] that will be compared with the stochastic simulations. However, in order to study qualitatively the phase diagrams and the stability of the solutions, we will use mean field equations obtained from the degree based approach in

which the correlations between the states of nodes and their neighbors are disregarded.

### A. Effective degree approach and mean field equations

For the effective degree approach, first introduced by Lindsquit *et al.* [5], the compartments are disaggregated by the states of the nodes of a network  $(\mathcal{A}, \mathcal{I}, \mathcal{E})$ , and by the number of its neighbors in each state. We denote by  $A(k_A, k_I, k_E)$  [and similarly  $I(k_A, k_I, k_E)$  and  $E(k_A, k_I, k_E)$ ] the density of active nodes (internal inactive and external inactive) with  $k_A$ ,  $k_I$  and  $k_E$  neighbors in state  $\mathcal{A}$ ,  $\mathcal{I}$  and  $\mathcal{E}$ , respectively; where  $k_A + k_I + k_E = k$  is the degree of a node. In our model, the flow into and outside these compartments are due to the change on the state of the nodes and their neighbors. The evolution equations for the states in our failure-recovery model are given by

$$\begin{aligned} \frac{dA(k_A, k_I, k_E)}{dt} = & \gamma_I I(k_A, k_I, k_E) + \gamma_E E(k_A, k_I, k_E) + \\ & -rA(k_A, k_I, k_E)\Theta(m - k_A) - pA(k_A, k_I, k_E) + \\ & \gamma_E[(k_E + 1)A(k_A - 1, k_I, k_E + 1) - k_E A(k_A, k_I, k_E)] + \\ & \gamma_I[(k_I + 1)A(k_A - 1, k_I + 1, k_E) - k_I A(k_A, k_I, k_E)] + \\ & p[(k_A + 1)A(k_A + 1, k_I - 1, k_E) - k_A A(k_A, k_I, k_E)] + \\ & rW_A[(k_A + 1)A(k_A + 1, k_I, k_E - 1) - k_A A(k_A, k_I, k_E)], \end{aligned} \quad (1)$$

$$\begin{aligned} \frac{dI(k_A, k_I, k_E)}{dt} = & -\gamma_I I(k_A, k_I, k_E) + pA(k_A, k_I, k_E) + \\ & \gamma_E[(k_E + 1)I(k_A - 1, k_I, k_E + 1) - k_E I(k_A, k_I, k_E)] + \\ & \gamma_I[(k_I + 1)I(k_A - 1, k_I + 1, k_E) - k_I I(k_A, k_I, k_E)] + \\ & p[(k_A + 1)I(k_A + 1, k_I - 1, k_E) - k_A I(k_A, k_I, k_E)] + \\ & +rW_I[(k_A + 1)I(k_A + 1, k_I, k_E - 1) - k_A I(k_A, k_I, k_E)], \end{aligned} \quad (2)$$

$$\begin{aligned} \frac{dE(k_A, k_I, k_E)}{dt} = & rA(k_A, k_I, k_E)\Theta(m - k_A) - \gamma_E E(k_A, k_I, k_E) + \\ & \gamma_E[(k_E + 1)E(k_A - 1, k_I, k_E + 1) - k_E E(k_A, k_I, k_E)] + \\ & +\gamma_I[(k_I + 1)E(k_A - 1, k_I + 1, k_E) - k_I E(k_A, k_I, k_E)] + \\ & p[(k_A + 1)E(k_A + 1, k_I - 1, k_E) - k_A E(k_A, k_I, k_E)] + \\ & rW_E[(k_A + 1)E(k_A + 1, k_I, k_E - 1) - k_A E(k_A, k_I, k_E)], \end{aligned} \quad (3)$$

where  $\Theta(x)$  is the Heaviside distribution. In these equations  $k_{\min} \leq k_A + k_I + k_E \leq k_{\max}$ , where  $k_{\min}$  and  $k_{\max}$  are the maximum and minimum degree of the degree distribution  $P(k)$ . Here,  $P(k)$  represents the fraction of nodes with  $k$  neighbors, *i.e.* with degree  $k$ .

Eq. (1) [and similarly Eqs. (2) and (3)] represents the evolution of the density of active nodes ( $I$  and  $E$ ) with  $k_A$ ,  $k_E$  and  $k_I$  neighbors in states  $\mathcal{A}$ ,  $\mathcal{I}$ ,  $\mathcal{E}$ , respectively [or with neighborhood  $(k_A, k_E, k_I)$ ]. Notice that the information of the degree distribution  $P(k)$  is encoded in the initial condition of the system of Eqs. (1)-(3). For example, for the initial condition in which all nodes are active,  $A(k_A = k, k_I = 0, k_E = 0) = P(k)$ .

In the r.h.s Eq. (1) the term:

- $\gamma_I I(k_A, k_I, k_E)$  represents the transition from a node in state  $\mathcal{I}$  with a neighborhood  $(k_A, k_I, k_E)$ , to state  $\mathcal{A}$ , due to the recovery of these inactive nodes,
- $\gamma_E E(k_A, k_I, k_E)$  corresponds to the transition from state  $\mathcal{E}$  to  $\mathcal{A}$  due to recovery at rate  $\gamma_E$ ,
- $r A(k_A, k_I, k_E)\Theta(m - k_A)$  depicts the density of active nodes with  $k_A \leq m$  that fail externally at a rate  $r$ ,
- $p A(k_A, k_I, k_E)$  represents the transition from nodes with state  $\mathcal{A}$  and neighborhood  $(k_A, k_I, k_E)$ , to nodes with state  $\mathcal{I}$  at a rate  $p$  due to internal failure,
- $p[(k_A + 1)A(k_A + 1, k_I - 1, k_E) - k_A A(k_A, k_I, k_E)]$  represents the transition, in which neighbors in state  $\mathcal{A}$  becomes  $\mathcal{I}$ ,
- $\gamma_E[(k_E + 1)A(k_A - 1, k_I, k_E + 1) - k_E A(k_A, k_I, k_E)]$  is the transition in which neighbors in state  $\mathcal{E}$  become active at a rate  $\gamma_E$ ,
- $\gamma_I[(k_I + 1)A(k_A - 1, k_I + 1, k_E) - k_I A(k_A, k_I, k_E)]$  represents the transition from neighbors in state  $\mathcal{I}$  to  $\mathcal{A}$  at a rate  $\gamma_I$ , and finally,
- $r W_A[(k_A + 1)A(k_A + 1, k_I, k_E - 1) - k_A A(k_A, k_I, k_E)]$  represents the density of active nodes whose neighbors in state  $\mathcal{A}$  become  $\mathcal{E}$ .

Here  $W_A$ , ( $W_I$  and  $W_E$ ) represents the probability that an active neighbor (with  $k_A \leq m$ ) is connected to a node in state  $\mathcal{A}$ , ( $\mathcal{I}$  and  $\mathcal{E}$ ) (see Fig. 2). Notice that the last four terms

depict the transitions of a node caused by its neighbors and not by changes in its own state.

In Table I we show the flow into and outside the compartment  $A(k_A, k_I, k_E)$  [see Eqs. (1)].

TABLE I: Transitions involved in Eq. (1).

Transition	Rate
$A(k_A, k_I, k_E) \rightarrow E(k_A, k_I, k_E)$	$-r$
$A(k_A, k_I, k_E) \rightarrow I(k_A, k_I, k_E)$	$-p$
$A(k_A, k_I, k_E) \rightarrow A(k_A + 1, k_I, k_E - 1)$	$-\gamma_E k_E$
$A(k_A, k_I, k_E) \rightarrow A(k_A + 1, k_I - 1, k_E)$	$-\gamma_I k_I$
$A(k_A, k_I, k_E) \rightarrow A(k_A - 1, k_I + 1, k_E)$	$-p k_A$
$A(k_A, k_I, k_E) \rightarrow A(k_A - 1, k_I, k_E + 1)$	$-r W_A k_A$
$I(k_A, k_I, k_E) \rightarrow A(k_A, k_I, k_E)$	$\gamma_I$
$E(k_A, k_I, k_E) \rightarrow A(k_A, k_I, k_E)$	$\gamma_E$
$A(k_A - 1, k_I, k_E + 1) \rightarrow A(k_A, k_I, k_E)$	$\gamma_E (k_E + 1)$
$A(k_A - 1, k_I + 1, k_E) \rightarrow A(k_A, k_I, k_E)$	$\gamma_I (k_I + 1)$
$A(k_A + 1, k_I - 1, k_E) \rightarrow A(k_A, k_I, k_E)$	$p (k_A + 1)$
$A(k_A + 1, k_I, k_E - 1) \rightarrow A(k_A, k_I, k_E)$	$r W_A (k_A + 1)$

It is straightforward the interpretation of each term of Eqs. (2) and (3). Note that the last relation in Table I represents an effective dynamical rate of transition at which active neighbors of an active node fail externally, which is proportional to  $W_A$ , that is, the ratio between the mean number of active neighbors of an active node that can fail and the total mean number of active neighbors:

$$W_A = \frac{\sum_{k_A=0}^m \sum_{k_I=0}^{k_{\max}} \sum_{k_E=0}^{k_{\max}} k_A A(k_A, k_I, k_E)}{\sum_{k_A=0}^{k_{\max}} \sum_{k_I=0}^{k_{\max}} \sum_{k_E=0}^{k_{\max}} k_A A(k_A, k_I, k_E)}. \quad (4)$$



Similarly  $W_I$ ,  $W_E$  are given by

$$W_I = \frac{\sum_{k_A=0}^m \sum_{k_I=0}^{k_{\max}} \sum_{k_E=0}^{k_{\max}} k_I A(k_A, k_I, k_E)}{\sum_{k_A=0}^{k_{\max}} \sum_{k_I=0}^{k_{\max}} \sum_{k_E=0}^{k_{\max}} k_I A(k_A, k_I, k_E)},$$

$$W_E = \frac{\sum_{k_A=0}^m \sum_{k_I=0}^{k_{\max}} \sum_{k_E=0}^{k_{\max}} k_E A(k_A, k_I, k_E)}{\sum_{k_A=0}^{k_{\max}} \sum_{k_I=0}^{k_{\max}} \sum_{k_E=0}^{k_{\max}} k_E A(k_A, k_I, k_E)}.$$

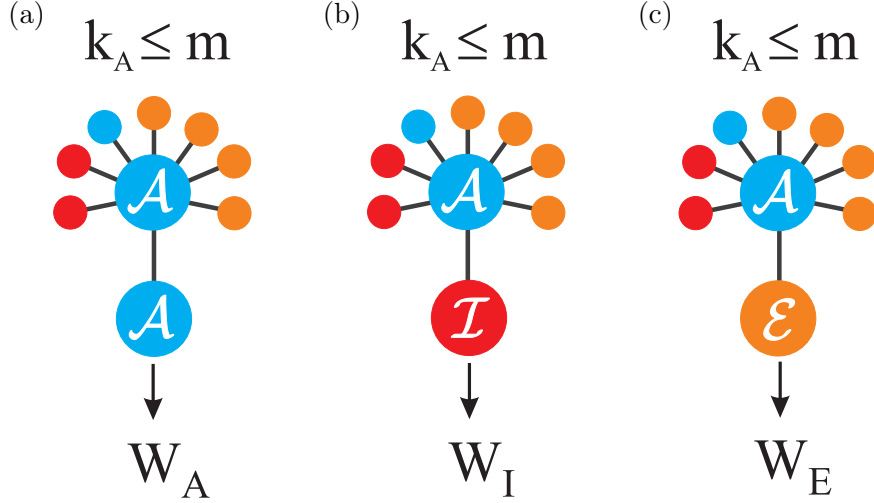


FIG. 2: Schematic representation of the terms  $W_A$  (a),  $W_I$  (b) and  $W_E$  (c) for  $m = 2$ . The colors of the nodes represent the same as in Fig. 1.  $W_A$  represents the fraction of edges connecting two active nodes, in which one of them has  $k_A \leq m$ . Similarly,  $W_I$  ( $W_E$ ) represents the fraction of edges connecting nodes in state  $\mathcal{I}$  ( $\mathcal{E}$ ) with nodes in state  $\mathcal{A}$  with  $k_A \leq m$ .

From the system of Eqs. (1)-(3) the density of nodes in states  $\mathcal{A}$ ,  $\mathcal{I}$  and  $\mathcal{E}$ , that we denote by  $A$ ,  $I$  and  $E$  respectively, are given by,

$$A \equiv \sum_{k_A=0}^{k_{\max}} \sum_{k_I=0}^{k_{\max}} \sum_{k_E=0}^{k_{\max}} A(k_A, k_I, k_E), \quad (5)$$

$$I \equiv \sum_{k_A=0}^{k_{\max}} \sum_{k_I=0}^{k_{\max}} \sum_{k_E=0}^{k_{\max}} I(k_A, k_I, k_E), \quad (6)$$

$$E \equiv \sum_{k_A=0}^{k_{\max}} \sum_{k_I=0}^{k_{\max}} \sum_{k_E=0}^{k_{\max}} E(k_A, k_I, k_E). \quad (7)$$

The agreement between Eqs. (1)-(3) and the simulations improves as the mean connectivity  $\langle k \rangle = \sum kP(k)$  increases. Therefore, in order to compare the effective degree equations with the stochastic model, in the following sections we present the results based on Random Regular (RR) networks, where all the nodes have the same degree  $z = 32$ , and in non-regular networks constructed using the Configurational Model [17] with  $\langle k \rangle = 32$ . For networks with a smaller mean connectivity ( $\langle k \rangle \approx 10$ ) we show only the simulations. In the stochastic model we use  $N = 10^6$  and the Gillespie's algorithm.

### III. RESULTS

#### A. Time evolution

We compute the density of nodes in state  $\mathcal{A}$ ,  $\mathcal{I}$  and  $\mathcal{E}$  in the steady state of our failure-recovery model as a function of  $p^* = 1 - \exp(-p/\gamma_I)$  (see Ref. [3]), which is a convenient parameter to show our numerical results since  $p^* \in [0, 1]$  ( $p^* = 0$  for  $p = 0$  and  $p^* = 1$  for  $p = \infty$ ). Additionally, for small values of  $p$  ( $p \ll \gamma_I$ ),  $p^*$  corresponds to the steady density of nodes in state  $\mathcal{I}$  of our model when  $r = 0$ , *i.e.* when there is no state  $\mathcal{E}$ , and nodes become  $\mathcal{A}$  and  $\mathcal{I}$  intermittently without any interaction between them (see Appendix A).

In Fig. 3, we show the evolution of the density of active nodes [see Eq. (5)] for RR network, obtained from the simulation and from Eqs. (1)-(3) for  $\gamma_I = 0.01$ ,  $\gamma_E = 1$ ,  $r = 5$ ,  $p^* = 0.40$  and  $m = 8$  for two different initial conditions,  $A = 1$  in (a) and  $I = 1$  in (b). Notice that  $A + E + I = 1$ .

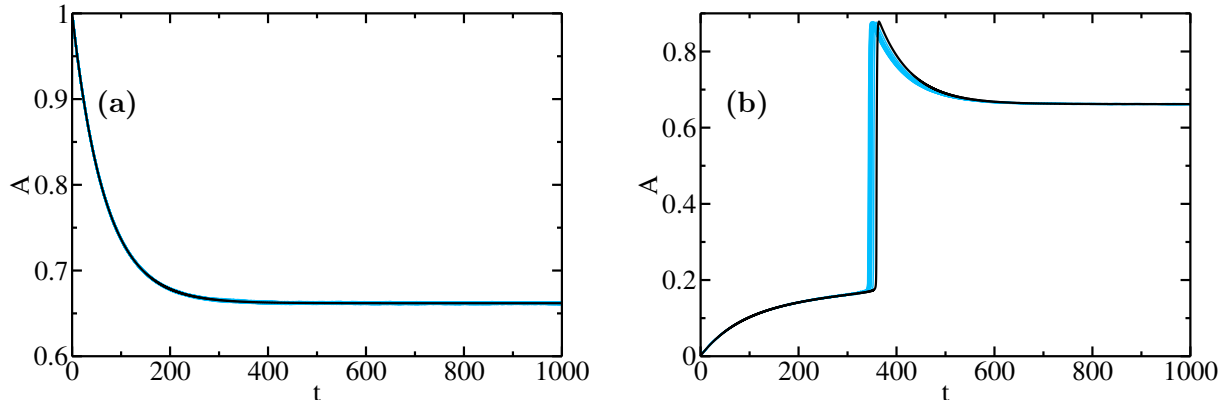


FIG. 3: Temporal evolution of the density of active nodes for RR networks with  $z = 32$  for  $\gamma_I = 0.01$ ,  $\gamma_E = 1$ ,  $r = 5$ ,  $m = 8$ ,  $p^* = 0.40$  for two initial conditions: (a)  $A = 1$  and (b)  $I = 1$ . The theoretical solutions (black) are obtained from the degree effective equations (1)-(3) and the simulations results (colored lines) are the results of 100 different network realizations with  $N = 10^6$ .

From Fig. 3 we can see that the theoretical model is in well agreement with the simulation. In Fig. 3 (b) we can see that there is a slightly difference between the simulations and the theory on the time at which the density of active nodes rises sharply. This difference can be explained by stochastic effects similarly than the one found in epidemic models [18] when the initial condition consists in a few infected nodes. For this case, the time at which the density of infected individuals grows sharply varies for different realizations [18]. For the parameters used in Fig. 3, the system reaches a steady state, however, we will show that for a specific region of parameters the system exhibits an oscillatory behavior, similarly to the ones found in some epidemic models [19–21] and in a model of neural networks [12]. In our model, these oscillations are a consequence of a competition between inactive internal nodes and inactive external nodes, with the aim of transforming the living nodes to their own state, as we will explain below.

In Fig. 4 (a), we plot the theoretical results for the evolution of the density of active nodes for the same parameters of Fig. 3(a), but for  $r = 3$ , instead of the value  $r = 5$  used in Fig. 3 for different values of  $p^*$ . From the figure we can see that the system exhibits oscillatory behavior in the range  $0.83 \leq p^* \leq 0.88$ .

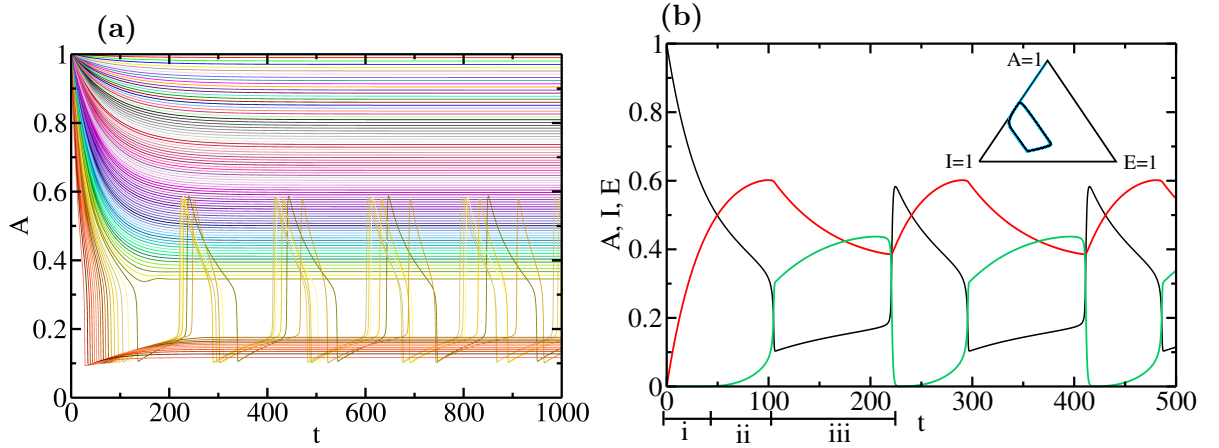


FIG. 4: For RR networks with  $\gamma_I = 0.01$ ,  $\gamma_E = 1$ ,  $r = 3$ ,  $m = 8$ : (a) density of active nodes as a function of time obtained from the effective degree approach for  $p^* = 1 - \exp(-p/\gamma_I)$  from 0.00 (top) to 0.99 (bottom) with  $\delta p^* = 10^{-2}$ ; and (b): temporal evolution of the density  $A$  (black),  $I$  (red) and  $E$  (green) with  $p = 0.01897$  ( $p^* = 0.85$ ) obtained from the effective degree approach. The intervals of time  $i$ ,  $ii$  and  $iii$  correspond qualitatively to different regimes due to the competition between nodes in state  $\mathcal{E}$  and  $\mathcal{I}$  (explained in the text). In the inset we show the phase portrait in a triangular simplex obtained from the main plot (black) and we compare the results with four stochastic network realizations (colored lines) with  $N = 10^6$  nodes.

The oscillatory phase can be explained as a competition between internal and external inactive nodes to turn active nodes into states  $\mathcal{I}$  and  $\mathcal{E}$ , respectively. The dynamic of this competition is shown in Fig. 4 (b) in which we identify qualitatively three consecutive regimes ( $i$ ,  $ii$  and  $iii$ ):

- ( $i$ ): Initially, in this interval all nodes are active and they can only fail internally because each active node has  $k_A > m$  neighbors. Therefore  $A$  goes down and  $I$  rises while  $E$  remains near to zero.
- ( $ii$ ): In this stage as  $I$  increases, the fraction of nodes in state  $\mathcal{E}$  raises faster than in the previous stage since there is an increasing number of active nodes with  $k_A \leq m$  neighbors. As these nodes in state  $\mathcal{A}$  become  $\mathcal{E}$ , there are less available active nodes that can make a transition to  $\mathcal{I}$  states, which is reflected in a slower increasing of  $I$ , until  $I$  reaches a maximum. Therefore in this stage, in the “competition” between

nodes in state  $\mathcal{E}$  and  $\mathcal{I}$  to turn active nodes into a new state, the external inactive nodes “win”.

- (iii): In this regime, the fraction of  $\mathcal{I}$  nodes decreases while the fraction of the  $\mathcal{E}$  ones is still growing. However since the external inactive nodes can recover more quickly than the internal inactive nodes ( $\gamma_E > \gamma_I$ ) the probability that  $k_A \leq m$  decreases. This implies that finally  $E$  reaches a maximum and then decreases very quickly, leaving active nodes available to fail internally and hence  $I$  grows, repeating again the behavior of stage (ii).

In the inset of Fig. 4 (b) we show, as an example, the results of the evolution of  $A$ ,  $I$  and  $E$  on a simplex triangle for different stochastic realizations with  $p^* = 0.85$ , which are in well agreement with the theoretical result. In Sec. IV we will study qualitatively this oscillatory behavior through a stability analysis and show how this regime depends on the parameters, using a mean field (MF) approach.

## B. Steady state

Another important feature of our dynamical model is the behavior of  $A$ ,  $I$  and  $E$  in the steady state (the non oscillatory region). In Fig. 5, we show the density of nodes in state  $\mathcal{A}$ ,  $\mathcal{I}$  and  $\mathcal{E}$  as a function of  $p^* = 1 - \exp(-p/\gamma_I)$  in the steady state for a random regular network. These curves are obtained from the evolution Eqs. (1)-(3) for  $\gamma_I = 0.01$ ,  $\gamma_E = 1$ ,  $m = 8$  for different values of  $r$  and initial condition  $A = 1$ . For  $r = 1$  [Fig. 5 (a)], we can see that as the effective rate of internal failure  $p^*$  increases, as expected, the density of nodes in state  $\mathcal{I}$  increases while for nodes in state  $\mathcal{A}$  decreases.

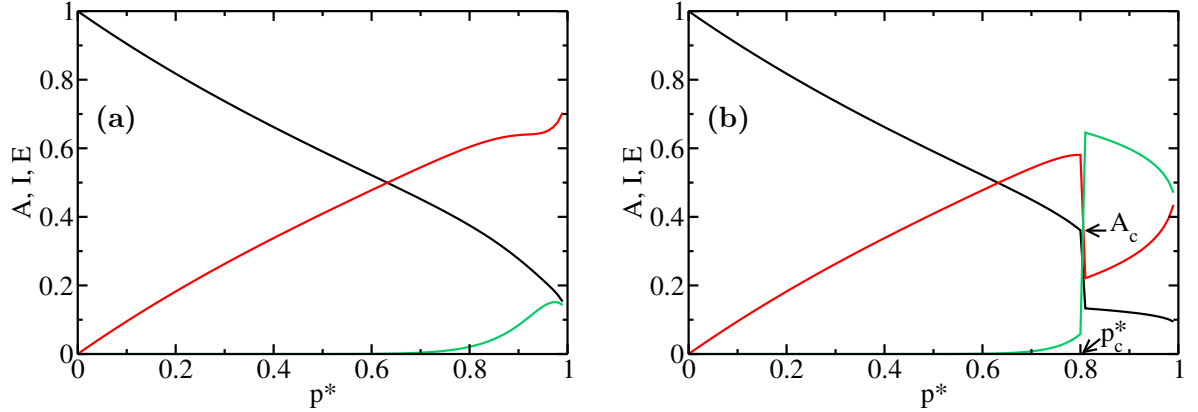


FIG. 5:  $A$  (black),  $I$  (red) and  $E$  (green) as a function of  $p^*$  for RR networks with  $\gamma_I = 0.01$ ,  $\gamma_E = 1$ ,  $m = 8$ , and (a)  $r = 1$  and (b)  $r = 5$  obtained from the effective degree approximation Eqs. (1)-(3). In Fig.(b),  $p_c^* = 0.81$  and  $A_c = 0.35$  is the fraction of active nodes for  $p^* = p_c^* - \delta p$ .  $A_c$  and  $p_c^*$  are denoted by arrows.

In Fig. 5 (b) we show the same curves as in Fig. 5 (a) for  $r = 5$ . As  $p^*$  increases from  $p^* = 0$  the curves behave similar to the case  $r = 1$ . However, at a certain value  $p^* \approx 0.81$ , denoted as the threshold  $p_c^*$ , we can see a sharp change in the curves, like in a first order phase transition, in which the density of nodes in states  $\mathcal{A}$  and  $\mathcal{I}$  abruptly goes down, while the density of  $\mathcal{E}$  grows sharply. As  $p^*$  increases, for  $p^* > p_c^*$  the density of nodes in state  $\mathcal{A}$  changes slower than for  $p^* < p_c^*$ . This implies that the variation in the density of nodes in state  $\mathcal{E}$  is transferred to the density of nodes in state  $\mathcal{I}$ , *i.e.*  $\mathcal{I}$  nodes win over  $\mathcal{E}$  for these parameters.

In order to assess the accuracy of the theoretical approach, in Fig. 6 we compare the theoretical results with the stochastic simulations for initial conditions  $A = 1$  and  $I = 1$ . We can see a good agreement between the effective degree approach and the simulations. For  $r = 5$  [see Fig. 6 (a)] we obtain theoretically a hysteresis region in the density of active nodes between  $p^* = 0.45$  and  $p^* = 0.81$ . In Sec. IV we will also study qualitatively the hysteresis through a stability analysis in the MF approximation.

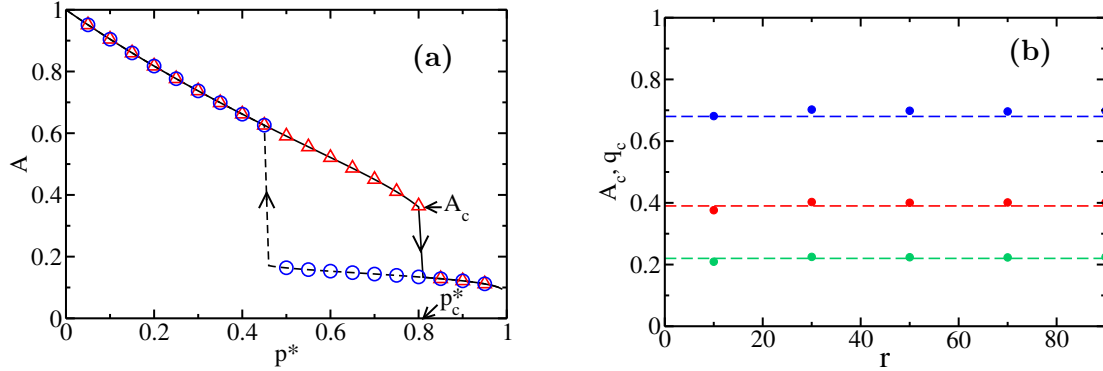


FIG. 6: Figure (a): Density of active nodes in the steady state as a function of  $p^*$  for RR networks with  $\gamma_I = 0.01$ ,  $\gamma_E = 1$ ,  $m = 8$  and  $r = 5$ . The lines were obtained from the effective degree approach. Dashed lines (solid lines) correspond to the case where the initial condition consists in all nodes in state  $\mathcal{I}$  (in state  $\mathcal{A}$ ). The symbols correspond to the stochastic simulations in which the initial condition is  $I = 1$  (blue circles) and  $A = 1$  (red triangles). The value of  $A_c$  is denoted by an horizontal arrow. The vertical arrows indicate the direction of the hysteresis loop. Figure (b): The steady fraction of active nodes  $A_c$  in our model (symbols) obtained from the Eqs. (1)-(3) as a function of  $r$  in RR networks for different values of  $m$ :  $m = 4$  (green),  $m = 8$  (red),  $m = 16$  (blue) for  $\gamma_I = 10^{-2}$  and  $\gamma_E = 1$ . We compare the values of  $A_c$  with the critical fraction of non-removed nodes in “random”  $k$ -core percolation  $q_c$  at which there is a first order transition that depends on  $m$ . The values of  $q_c$  are displayed by dashed lines with the same colors as  $A_c$ . To compute the value of  $A_c$  for each value of  $r$ , we evaluate the final fraction of active nodes for  $p^* \in (0, 1)$  with  $\delta p^* = 10^{-2}$ , and then choose the value of  $p^* = p_c^*$  above which there is a sharp decrease in  $A$ .

The observed sharp drop in the density of active nodes for the initial condition  $A = 1$  close to  $p_c^*$  [see Fig. 6 (a)], in the theory and simulations, is reminiscent of the first order transition found in “random”  $k$ -core percolation [13]. In the latter process there is a critical initial fraction of removed nodes (similar to inactive nodes in our spontaneous failure-recovery model) that triggers a sharp decrease in the fraction of living nodes (as mentioned in Sec. II and Appendix B1). Interestingly, we find a similitude between our model and “random”  $k$ -core percolation because the value of the steady fraction of active nodes just before the first order transition (with initial condition  $A = 1$ ), denoted by  $A_c$ ,

is near to the critical value of the control parameter  $q$  of this percolation process.

In Fig. 6 (b) we plot the value of  $A_c$  for  $p^* = p_c^* - \delta p^*$  (*i.e.* just before  $A$  goes down sharply) for different values of  $r$  and  $m$  obtained from the evolution Eqs. (1)-(3) and we compare them with the threshold value  $q_c$  in  $k$ -core percolation for the same values of  $m$  (see equations in Appendix B1). From the figure we can see that the values of  $q_c$  predicted by the “random”  $k$ -core process at which a giant component disappears are in well agreement with the values  $A_c$  obtained from our failure-recovery model in RR networks.

In these networks the relation between the failure-recovery model and the “random”  $k$ -core arises from the fact that all the nodes have the same connectivity, and then they have the same probability to be active. In Appendix B2 we explain with more detail this relation. On the other hand, for a constant value of  $m$ , if we consider the case of a broader degree distribution, such as a truncated Poisson degree distribution

$$P(k) = c \frac{e^{-\lambda} \lambda^k}{k!} \Theta(k - k_{\min}) \Theta(k_{\max} - k), \quad (8)$$

in which  $c$  is a normalization constant [see Fig. 7(a)], we also obtain that the steady value of  $A$  just before the fraction of active nodes drops to zero is near the predicted one from “random”  $k$ -core percolation, in particular for lower values of  $m$ . Additionally, in Fig. 7 (b) we plot the probability that a node is active, given that it has connectivity  $k$ . We can see that nodes with  $k = k_{\min}$  have the lowest probability to be active. Nevertheless, the fact that for this network  $1 - P(k_{\min}) = 0.86$  and besides that the probability that a node is active remains nearly constant disregarding its connectivity, imply that “random”  $k$ -core percolation predicts approximately the value of  $A_c$ . However, as we will show below, if we consider a higher heterogeneity on the connectivities of the nodes than in the previous case, we obtain that the steady state of the process can be better described by a “targeted”  $k$ -core process rather than by the “random”  $k$ -core percolation.



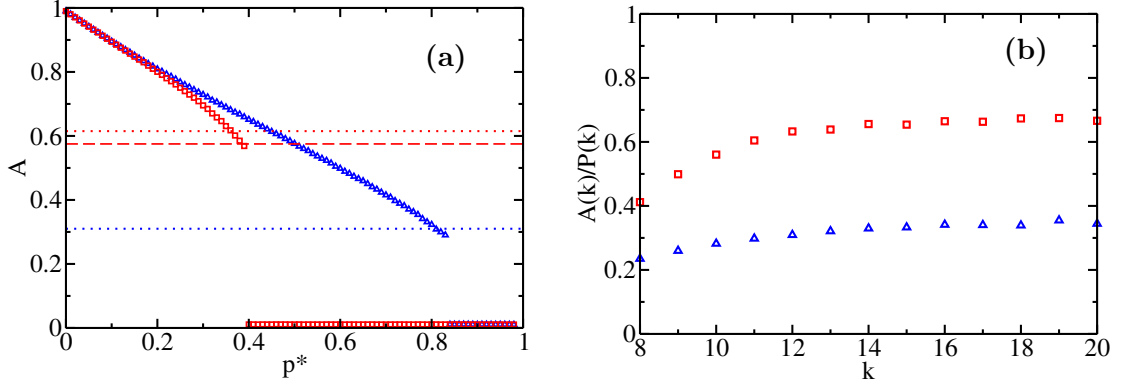


FIG. 7: Figure (a): Density of active nodes in the steady state as a function of  $p^*$  obtained from the simulations for a network with a truncated Poisson distribution [see Eq. (8)] with  $k_{\min} = 8$ ,  $k_{\max} = 20$  and  $\lambda = 10$  and for  $\gamma_I = 0.01$ ,  $\gamma_E = 1$ ,  $r = 90$ ,  $m = 2$  (blue triangles) and  $m = 4$  (red squares). The dotted lines correspond to the value of  $q_c$  predicted by the “random”  $k$ -core percolation, at which the fraction of active nodes would drop to zero if active nodes were homogeneously distributed. The dashed line corresponds to the value of  $q_c$  obtained from Eqs. (B3) and (B5), and using the steady distribution of active nodes  $q_k$  [see Eq. (B6)] obtained just before the fall of  $A$ . This is explained in the end of Sec. III B. Figure (b): Steady fraction  $A(k)$  of active nodes of connectivity  $k$  relative to  $P(k)$ , obtained from the simulations just before the fall of  $A$ . Blue symbols correspond to the case  $m = 2$  and the red ones to  $m = 4$ .

In Fig. 8 (a) we show the steady fraction of active nodes as a function of  $p^*$  for a bimodal network with connectivities  $k = 20$ ,  $k = 40$  and mean connectivity  $\langle k \rangle = 32$  for  $m = 16$ . From the figure we can see that for the initial condition  $A = 1$ , the system can exhibit two transitions for high enough value of  $m$ . This is expected since as  $p^*$  increases, after the first sharp transition the nodes with the lowest connectivity will fail, while the nodes with the largest connectivity will remain active [see inset of Fig. 8(a)]. Therefore, just before the second transition ( $p^* \lesssim 0.30$ ) the distribution of active nodes is not homogeneous, and as a consequence the “random”  $k$ -core percolation is not appropriate to describe the steady state. For this case, in Appendix B 3 we present the equations of the “targeted”  $k$ -core percolation that takes into account the inhomogeneous distribution of active nodes that we will use to compute  $q_c$ . In Fig. 8 (b) we compare  $A_c$  with the value of  $q_c$  obtained following Appendix B 3, for a bimodal network for different values of  $m$  and  $r$ .

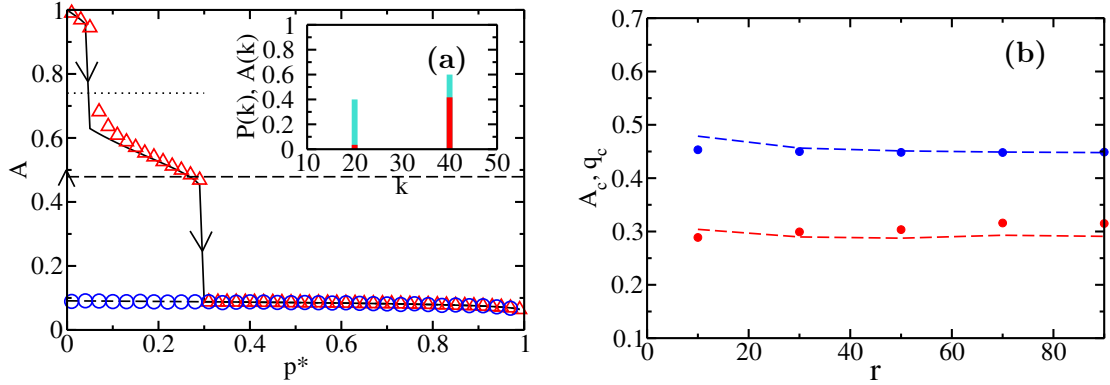


FIG. 8: Figure (a): Density of active nodes in the steady state as a function of  $p^*$  for a bimodal network with connectivities  $k = 20$  and  $k = 40$  with  $\langle k \rangle = 32$  for  $\gamma_I = 0.01$ ,  $\gamma_E = 1$ ,  $m = 16$  and  $r = 10$ . The solid lines were obtained from the effective degree approach. The symbols and solid lines have the same meaning as in Fig. 6. The dotted line corresponds to the value of  $q_c$  predicted by the “random” k-core percolation. The dashed line corresponds to the value of  $q_c$  obtained from Eqs. (B3) and (B5), and using the steady distribution of actives nodes  $q_k$  [see Eq. (B6)] obtained just before the second fall of  $A$ . In the inset we show the bar graphic of  $P(k)$  (light blue), and  $A(k)$  (red) measured in the steady state just before the second fall. Figure (b): The steady fraction of active nodes  $A_c$  in our model (symbols) obtained from the Eqs. (1)-(3) as a function of  $r$  in bimodal networks for different values of  $m$ :  $m = 8$  (red) and  $m = 16$  (blue) for  $\gamma_I = 10^{-2}$  and  $\gamma_E = 1$ . Dashed lines were obtained using Eqs. (B3)-(B6) as explained in the main text.

From the figure we can see that the values of  $q_c$  predicted by the “targeted” k-core process at which the giant component disappears are in well agreement with the values  $A_c$  obtained from our failure-recovery model in bimodal networks. Additionally, using “targeted” k-core percolation, we also compute the value of  $q_c$  for the truncated Poisson distribution [see dashed line in Fig. 7(a)] with  $m = 4$ ; in which we obtain that this value is closer to  $A_c$  than the one obtained by “random” k-core percolation. Therefore, these results suggest that the equations of “targeted” k-core percolation could be considered in non-regular networks and used as a benchmark to compare the results with a failure-recovery model.

In the following section we will show, using the mean field approach, the region of

parameters where the system has hysteresis and oscillatory behaviors.

#### IV. STABILITY ANALYSIS THROUGH MEAN FIELD EQUATIONS

##### A. Deduction of Mean Field equations

In order to study the oscillating and hysteresis regions of our failure-recovery spontaneous model, we use the mean field equation (MF) derived from the effective degree approach. In particular for RR networks, these equations depict a dynamics in which nodes shuffle their links instantaneously [22]. While in this approach the information about the structure of the network is lost, we can estimate the region of parameters where the hysteresis and the oscillatory phase exist.

Adding the system of Eqs. (1)-(3) over  $k_A$ ,  $k_I$  and  $k_E$ , we obtain the following equations

$$\frac{dA}{dt} = \gamma_I I + \gamma_E E - r \sum_{k_A=0}^m \sum_{k_I=0}^{k_{\max}} \sum_{k_E=0}^{k_{\max}} A(k_A, k_I, k_E) - pA, \quad (9)$$

$$\frac{dI}{dt} = -\gamma_I I + pA, \quad (10)$$

$$\frac{dE}{dt} = r \sum_{k_A=0}^m \sum_{k_I=0}^{k_{\max}} \sum_{k_E=0}^{k_{\max}} A(k_A, k_I, k_E) - \gamma_E E. \quad (11)$$

Notice that these equations do not depend on  $W_A$ ,  $W_I$ ,  $W_E$  because the terms with these coefficients cancel each other after the addition of the equations mentioned above. Since  $A + I + E = 1$ , the evolution equations can be written as

$$\frac{dA}{dt} = \gamma_I I + \gamma_E (1 - A - I) - r \sum_{k_A=0}^m \sum_{k_I=0}^{k_{\max}} \sum_{k_E=0}^{k_{\max}} A(k_A, k_I, k_E) - pA, \quad (12)$$

$$\frac{dI}{dt} = -\gamma_I I + pA. \quad (13)$$

Using a mean field approximation, the third term of Eq. (12) can be approximated by

$$\sum_{k_A=0}^m \sum_{k_I=0}^{k_{\max}} \sum_{k_E=0}^{k_{\max}} A(k_A, k_I, k_E) = A \sum_{k=k_{\min}}^{k_{\max}} P(k) \sum_{k_A=0}^m \binom{k}{k_A} (1-A)^{k-k_A} A^{k_A}, \quad (14)$$

and thus the evolution equations in the MF approach are given by

$$\frac{dA}{dt} = \gamma_I I + \gamma_E (1 - A - I) - rA \sum_{k=k_{\min}}^{k_{\max}} P(k) \sum_{k_A=0}^m \binom{k}{k_A} (1-A)^{k-k_A} A^{k_A} - pA, \quad (15)$$

$$\frac{dI}{dt} = -\gamma_I I + pA. \quad (16)$$

At the steady state of the process  $dA/dt = dI/dt = 0$ , and thus  $A$  satisfies the following self-consistent equation [obtained from Eqs. (15) and (16)]

$$A = \left(1 - \frac{p}{\gamma_I} A\right) - \frac{r}{\gamma_E} A \sum_{k=k_{\min}}^{k_{\max}} P(k) \sum_{k_A=0}^m \binom{k}{k_A} (1-A)^{k-k_A} A^{k_A}. \quad (17)$$

Despite that in the steady state the value of  $A$  depends only on the ratios  $p/\gamma_I$  and  $r/\gamma_E$ , the stability of the solutions or fixed points depends on the individual values of the parameters. In order to study the stability of the fixed points we linearize the equations (15) and (16) around the fixed points obtained from Eq. (17) and compute the eigenvalues of the Jacobian matrix evaluated at the steady state [23].

In the following we will analyze the stability of the solutions in the steady state for  $\gamma_I < \gamma_E$  and  $\gamma_I > \gamma_E$ , and show that only for  $\gamma_I < \gamma_E$ , the system can sustain oscillations.

## B. Steady states for $\gamma_I < \gamma_E$

In Fig. 9 we show the stability of the solutions of the density of active nodes for different values of  $r$  for RR networks with  $z = 32$ ,  $\gamma_I = 0.01$ ,  $\gamma_E = 1$ ,  $m = 8$ .

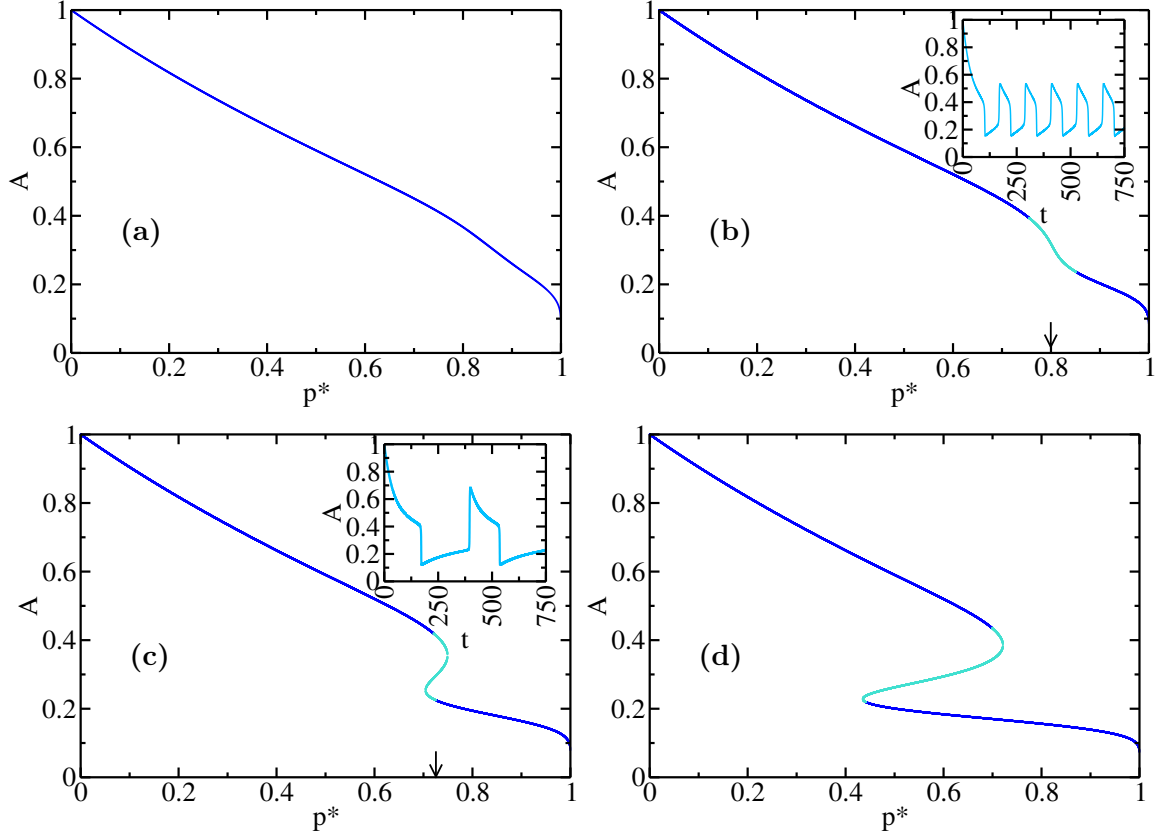


FIG. 9: Steady state of  $A$  as a function of  $p^*$  for a RR network with  $\gamma_I = 0.01$ ,  $\gamma_E = 1$ ,  $m = 8$  and  $r = 1$  (a),  $r = 2$  (b),  $r = 3$  (c) and  $r = 4$  (d). The curves represent the fixed points obtained from Eq. (17). Colored lines represent different stability-regimes obtained from the eigenvalues of the system of Eqs. (15) and (16): light blue (unstable) and blue (stable). In the insets of figures (b) and (c) we show the temporal evolution of the average density of active nodes [obtained from Eqs. (15) and (16)] for the values of  $p^*$  indicated by the arrow.

We observe that for  $r = 1$ , [see Fig. 9(a)] there is only one stable fixed point of Eq. (17) for each value of  $p^*$ . As  $r$  increases to  $r = 2$  and  $r = 3$ , for a range of values of  $p^*$  the fixed points of Eq. (17) are all unstable, and therefore the densities oscillate [24] [see figures 9(b) and 9(c)], *i.e.* an oscillatory regime appears for the case  $\gamma_I < \gamma_E$ , as observed also in the effective degree formalism (see Fig. 4). Finally, for the largest value of  $r$  [ $r = 4$ , see figure 9(d)] a hysteresis region appears, *i.e.* there are two stable fixed points of Eq. (17)

for some values of  $p^*$ .

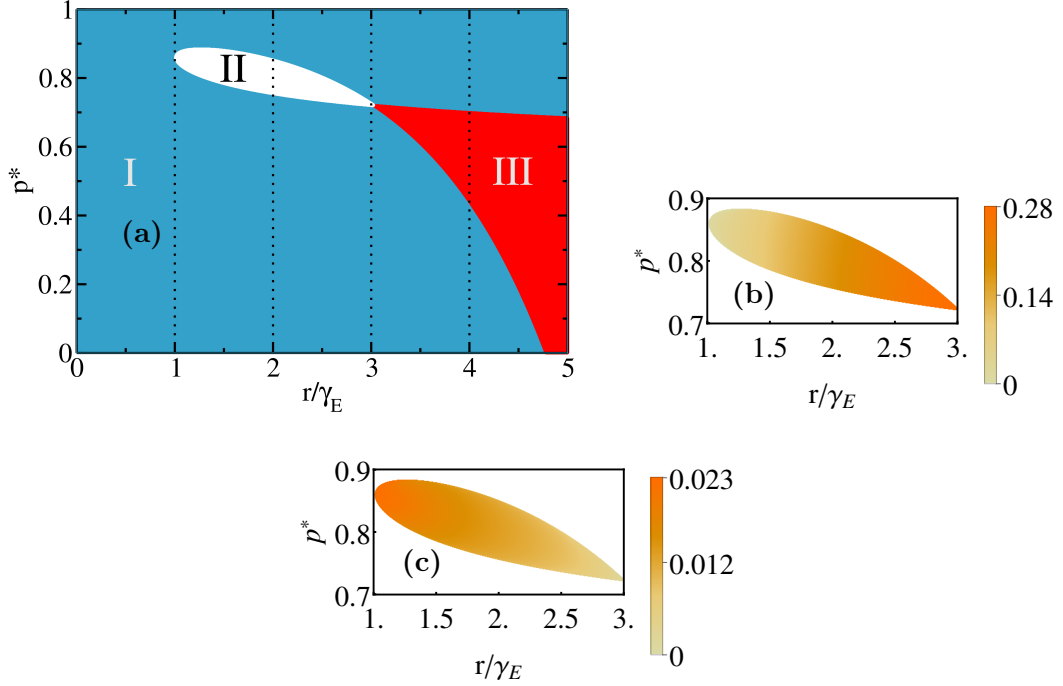


FIG. 10: Figure (a): phase diagram in the plane  $p^*$ - $r/\gamma_E$  for  $\gamma_E = 1$  and  $\gamma_I = 0.01$ . The region I (blue) corresponds to one fixed point of the fraction of active nodes, region II (white) corresponds to an oscillatory regime and region III (red) depicts the parameters of the hysteresis region. The vertical dotted lines correspond to the paths on the phase diagram studied in Fig. 9. Figure (b): the amplitude of the oscillations in region II of figure (a). Figure (c): frequency (computed as  $1/T$ , where  $T$  is the period) of the oscillations in region II of figure (a).

Notice that the mean field equations (15) and (16) qualitatively captures all the regimens observed in our model for the case  $\gamma_I < \gamma_E$ . In Fig. 10(a) we show the three regimens in the plane  $p^*$ - $r/\gamma_E$  in which the oscillatory region is bounded but not negligible. Therefore the oscillatory behavior is robust in a scenario at which the parameters can vary slightly over time within this region. This is an important fact for biological systems in which sustained oscillations are present [25–29]. In order to study the dependency of the amplitude and the frequency on the parameters, we measure directly these magnitudes from the integration of Eqs. (15) and (16). In Figs. 10 (b) and (c) we plot the amplitude

and frequency respectively, which shows that for larger values of  $r/\gamma_E$  the system oscillates slower but with a higher amplitude, which is consistent with the fact that the parameters are close to the hysteresis region [see region III in Figs. 10(a)]. Furthermore, we observe that in this system the amplitude of the oscillations can be suppressed abruptly when crossing the transition line, from region II to I. Finally, we obtain that the frequency and the amplitude are more sensible under variations in  $r/\gamma_E$  than under variations of  $p^*$ . This result is compatible with the shape of the oscillations, shown in Fig. 4(a), which have similar amplitudes and frequencies for different values of  $p^*$ .

### C. Steady regimes for $\gamma_I > \gamma_E$

In order to study the steady state for  $\gamma_I > \gamma_E$  we will construct the Lyapunov function  $V(A, I)$  which allows to study the global stability of a system. The Lyapunov function can only be used if its derivative with respect to time is negative [30]. In order to achieve this goal, we next show that the dynamical Eqs. (15) and (16) can be expressed as a non-gradient flow [30], *i.e.*

$$\frac{dA}{dt} = -a \frac{\partial V(A, I)}{\partial A}, \quad (18)$$

$$\frac{dI}{dt} = -b \frac{\partial V(A, I)}{\partial I}, \quad (19)$$

where  $a$  and  $b$  are unknown positive constants whose values should be consistent with Eqs. (15)-(16). Here, we use without loss of generality,  $b = 1$ .

After matching the right hand side of Eqs. (18)-(19) with Eqs. (15)-(16) and integrating, the Lyapunov function  $V(A, I)$  can be written as

$$V(A, I) = \gamma_I \frac{I^2}{2} - pIA + \frac{p}{\gamma_I - \gamma_E} \left[ p \frac{A^2}{2} - \gamma_E \left( A - \frac{A^2}{2} \right) + r \sum_{k=k_{\min}}^{k_{\max}} \sum_{k_A=0}^m \sum_{j=0}^{k-k_A} P(k) \binom{k}{k_A} \binom{k-k_A}{j} (-1)^j \frac{A^{k_A+j+2}}{k_A+j+2} \right], \quad (20)$$

where

$$a = \frac{\gamma_I - \gamma_E}{p}, \quad (21)$$

with  $\gamma_I > \gamma_E$  (in order to ensure that  $a > 0$ ). Using the proposed Lyapunov function and the values of  $a$  and  $b$ , it is straightforward to show that these values allows to reconstruct

Eqs. (15)-(16) through Eqs. (18)-(19). In Fig. 11, we plot the Lyapunov function for  $\gamma_E = 0.01$  and  $\gamma_I = 1$ . From the plot we can see that the Lyapunov function has two local minimums.

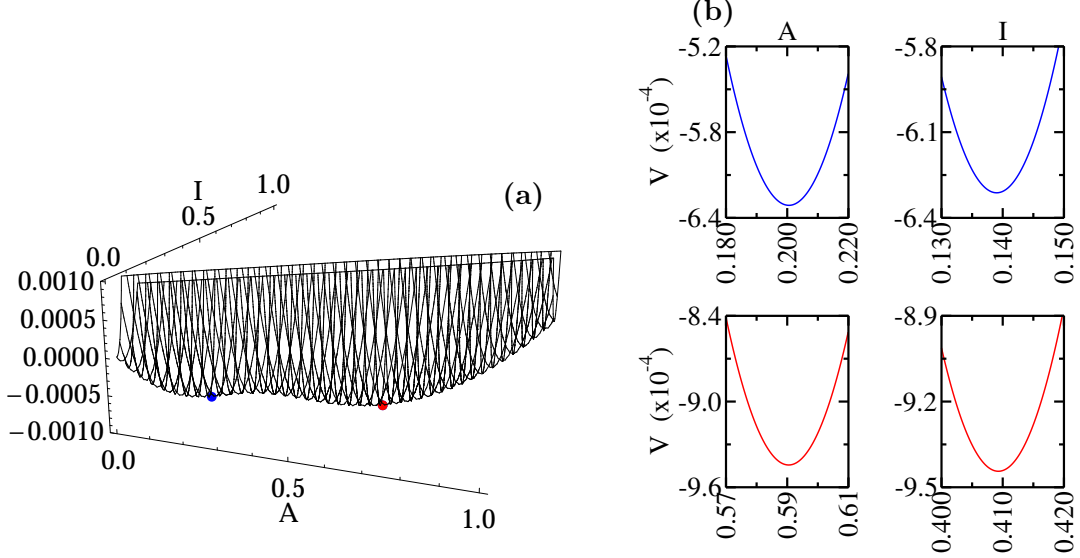


FIG. 11: (a): Lyapunov function as a function of  $A$  and  $I$  for  $p^* = 0.50$  and  $r = 4$  for  $m = 8$ ,  $\gamma_I = 1$  and  $\gamma_E = 0.01$  in a RR network. The red and blue points correspond to the local minimums of this function. Figure (b): Projection of the function around the local minimums of Fig.(a) in the plane  $V - A$  and  $V - I$ .

For  $\gamma_I > \gamma_E$ ,  $dV(A, I)/dt < 0$ , and therefore the overall system tends to a local minimum. In addition, since  $V(A, I)$  is expressed in terms of powers of  $A$  and  $I$ , it has a finite number of local and isolated minimums, hence an oscillatory behavior is not allowed because the system get stuck in a local minimum, from which it cannot escape due to the lack of fluctuations. Notice that in the case  $\gamma_I < \gamma_E$ , we cannot use the Lyapunov function given by Eq. (20), since for this case the parameter  $a$  in Eq. (18) is negative. This implies that we cannot guarantee that  $dV(A, I)/dt < 0$ , and therefore the dynamics of the system is not necessarily in a minimum of the function  $V(A, I)$ .

In Fig. 12 we show the phase diagram in the plane  $p^* - r/\gamma_E$  for the case  $\gamma_I > \gamma_E$ , obtained from Eq. (17). We can see that in region I there is only one stable fixed point, while in region II there are two stable fixed points, *i.e.*, the hysteresis behavior is present, especially for large values of  $r/\gamma_E$ . However, there is not an oscillatory regime, which is compatible with the existence of a Lyapunov function. Therefore, the relation between  $\gamma_E$



and  $\gamma_I$  is a key factor for the existence of sustained oscillations but not for the hysteresis.

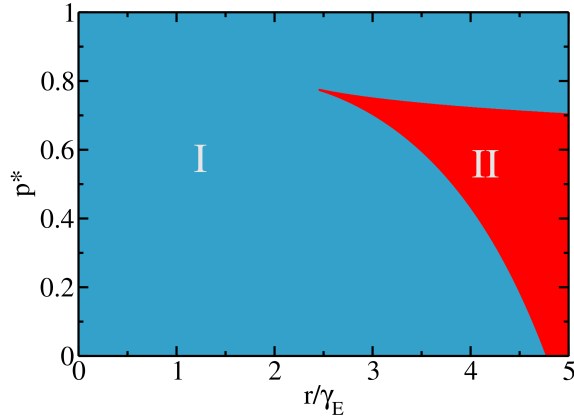


FIG. 12: Phase diagram  $p^*$  vs.  $r$  for  $m = 8$ ,  $\gamma_I = 1$  and  $\gamma_E = 0.01$  in a RR network. Region I (blue) corresponds to the existence of a single value of the fraction of active nodes in the steady state and region II (red) depicts the parameters of the hysteresis region.

## V. CONCLUSION

In summary, in this work we study a failure-recovery model in which the failure state belongs to two different kinds: internal and external failed nodes. Using the degree effective approach and simulations we found theoretically and via stochastic simulations that the system may exhibit hysteresis on the fraction of active nodes and also an oscillatory behavior as a result of the competition between external and internal inactive nodes. In the steady state we find that in random regular networks, the critical fraction of active nodes below which there is an abrupt collapse is close to the threshold in the “random”  $k$ -core percolation. However for non-regular networks, the topology can lead to an inhomogeneous distribution of active nodes which can be better described by “targeted”  $k$ -core percolation rather than by a “random”  $k$ -core percolation. Using a MF approach, we obtain that for  $\gamma_E > \gamma_I$  there is a range of the parameters at which the system can exhibit sustained oscillations, and that their amplitude increases and their frequency decreases as the parameters approach to the region at which hysteresis is present. Finally we show through the Lyapunov function that for  $\gamma_I > \gamma_E$ , the oscillatory phase is absent but can still exist a hysteresis region. We believe that the model we proposed and the equations developed in this work can be the useful for future research on dynamical systems and

their relation with percolation theory. A possible extension of our model would be to generalize our equations to take into account heterogeneous values of  $m$ . Another possible extension could be to model the process in interacting networks [31] which could allow to understand how the transitions can be affected by the interaction.

## Appendix A: Derivation of $p^*$

In this section, we obtain the parameter  $p^*$  as the steady fraction of inactive internal nodes when  $\gamma_E = r = 0$ , which corresponds to the case in which the nodes on the network can only be in states  $\mathcal{A}$  and  $\mathcal{I}$ .

For the case  $\gamma_E = r = 0$  the nodes activate and fail intermittently without interaction between them and therefore, the temporal evolution of the fraction of nodes in state  $\mathcal{A}$  and  $\mathcal{I}$  is governed by the following equations,

$$\frac{dA}{dt} = \gamma_I I - p A, \quad (\text{A1})$$

$$\frac{dI}{dt} = -\gamma_I I + p A. \quad (\text{A2})$$

Notice that we are assuming as initial condition of the dynamics that there are no externally failed nodes. Since  $E \equiv 0$ , then  $I + A = 1$  and the Eq. (A2) reduces to,

$$\frac{dI}{dt} = -\gamma_I I + p (1 - I), \quad (\text{A3})$$

whose solution in the steady state is given by,

$$I(t \rightarrow \infty) = \frac{p}{\gamma_I + p}. \quad (\text{A4})$$

For small values of  $p$ , the last expression can be rewritten as,

$$I(t \rightarrow \infty) \approx \frac{p}{\gamma_I} \approx 1 - \exp\left(-\frac{p}{\gamma_I}\right) \equiv p^*. \quad (\text{A5})$$

## Appendix B: k-core Percolation

### 1. “Random” k-core Percolation

Random  $k$ -core percolation is an irreversible dynamical process in which a node can be removed (dead) or non-removed (living). In the initial state, all nodes are living and

then a randomly fraction  $1 - q$  of nodes is removed. Afterwards, all the living nodes with  $m$  or less living neighbors, are removed. This step is repeated iteratively until the system is composed only by living nodes with more than  $m$  living neighbors. In Ref. [13], using a generating function formalism, the steady state of the final fraction of living nodes in complex networks  $P_\infty$ , was described by solving the following self-consistent equation

$$Q_\infty = 1 - q + q \sum_{k=k_{\min}}^{k_{\max}} \frac{kP(k)}{\langle k \rangle} \sum_{u=0}^{m-1} \binom{k-1}{u} Q_\infty^{k-1-u} (1 - Q_\infty)^u, \quad (\text{B1})$$

where  $Q_\infty$  is the probability of reaching a dead node through a randomly chosen link. The value of  $Q_\infty$  that depends on  $q$  is found solving the self-consistent equation (B1) in  $Q_\infty$ .

With the solution of  $Q_\infty$  for a given value of  $q$ , we obtain the fraction of nodes in the giant component  $P_\infty$ :

$$P_\infty = q \sum_{k=k_{\min}}^{k_{\max}} P(k) \left( 1 - \sum_{u=0}^m \binom{k}{u} Q_\infty^{k-u} (1 - Q_\infty)^u \right). \quad (\text{B2})$$

## 2. Relation between the failure-recovery model in RR networks and “random” $k$ -core percolation

In order to explain the similitude between  $A_c$  and  $q_c$  for RR networks, discussed in Sec. IIIB [see Fig. 6 (b)], in Fig. 13 we plot the simulations for: (i)  $A$ , (ii) the fraction of active nodes with  $k_A \leq m$  ( $A_m$ ) and (iii) the fraction of active nodes that belong to the GC ( $A_{GC}$ ) as a function of  $p^*$ .

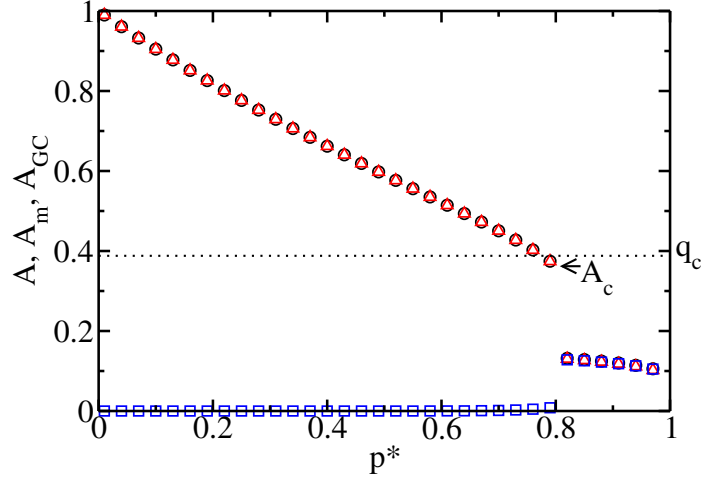


FIG. 13:  $A$  (black,  $\circ$ ),  $A_m$  (blue,  $\square$ ) and  $A_{GC}$  (red,  $\triangle$ ) as a function of  $p^*$  obtained from simulations for  $m = 8$ ,  $r = 10$ ,  $\gamma_I = 10^{-2}$  and  $\gamma_E = 1$  with  $N = 10^5$ . The dotted line indicates  $q_c = 0.38$  and the arrow indicates  $A_c = 0.36$ .

From the figure, we can see that for  $A > A_c$  almost all active nodes belong to the GC with  $k_A > m$  while for  $A < A_c$  almost all active nodes have  $k_A \leq m$ . Heuristically, in a k-core percolation framework, these results can be interpreted in the following way: assuming that the total fraction of active nodes at which  $A \sim A_c \cong q_c$  are placed randomly on the network, k-core percolation predicts the existence of a GC with active nodes with at least  $k_A > m$  neighbors, which avoids the collapse of the system. If the fraction of active nodes is below  $A_c$  this GC with active nodes with  $k_A > m$  does not exist. Therefore, if the system has a large value of  $r$  (*i.e.* if the rate at which  $\mathcal{A}$  goes to  $\mathcal{E}$  is large compared to the rate of recovery  $\gamma_E$ ), then the fraction of external inactive nodes rises sharply and  $A$  collapses. Therefore for large values of  $r$ , k-core percolation theory allows to estimate approximately the value of active nodes below which there is a first order transition.

### 3. Targeted k-core percolation

Given a network with degree distribution  $P(k)$ , let  $1 - q_k$  be the probability that a node with degree  $k$  is initially removed on the cascade of failure in a k-core percolation process. Then, following Ref. [32], it is straightforward to show that the final fraction of

non-removed nodes is obtained solving the following equations,

$$Q_\infty = \sum_{k=k_{\min}}^{k_{\max}} \frac{kP(k)}{\langle k \rangle} \left( 1 - q_k + q_k \sum_{u=0}^{m-1} \binom{k-1}{u} Q_\infty^{k-1-u} (1 - Q_\infty)^u \right), \quad (\text{B3})$$

$$P_\infty = \sum_{k=k_{\min}}^{k_{\max}} P(k) q_k \left( 1 - \sum_{u=0}^m \binom{k}{u} Q_\infty^{k-u} (1 - Q_\infty)^u \right), \quad (\text{B4})$$

where  $Q_\infty$  is the probability of reaching a removed node through a link. In this “targeted” k-core percolation process, likewise as in the “random” k-core percolation, we also called  $q$  the total initial fraction of non-removed nodes, *i.e.*

$$q = \sum_{k=k_{\min}}^{k_{\max}} P(k) q_k. \quad (\text{B5})$$

In the “random” k-core percolation process, a variation in the value of  $q$  implies that the fraction of non-removed nodes varies in the same proportion independent of its connectivity. However in the “targeted” k-core percolation process, there is not a unique way to change the fraction  $q_k$ . Therefore we propose that for a given distribution of  $q_k$  which satisfies Eq. (B5), a decreasing on the value of  $q$  implies that the distribution  $q_k$  decreases from its tail, *i.e.* the non-removed nodes with the highest connectivity are removed. A similar process is performed when the value of  $q$  is increased. Then we propose that in the steady state of our failure-recovery model for heterogeneous degree distributions,  $q_k$  is given by

$$q_k = \sum_{k_A=k_{\min}}^{k_{\max}} \sum_{k_I=k_{\min}}^{k_{\max}} \sum_{k_E=k_{\min}}^{k_{\max}} A(k_A, k_I, k_E) \delta_{k, k_A+k_I+k_E} \quad (\text{B6})$$

In order to show that for  $A = A_c$ , this distribution of non-removed nodes is near a transition point in a “targeted” percolation process, we vary the value of  $q$  [given by Eq. (B5)] starting from the distribution  $q_k$  [see Eq. (B6)] as explained above, in order to compute  $q_c$ . In Fig. 14 we summarize with a schematic, the steps to compute the value of  $q_c$ .

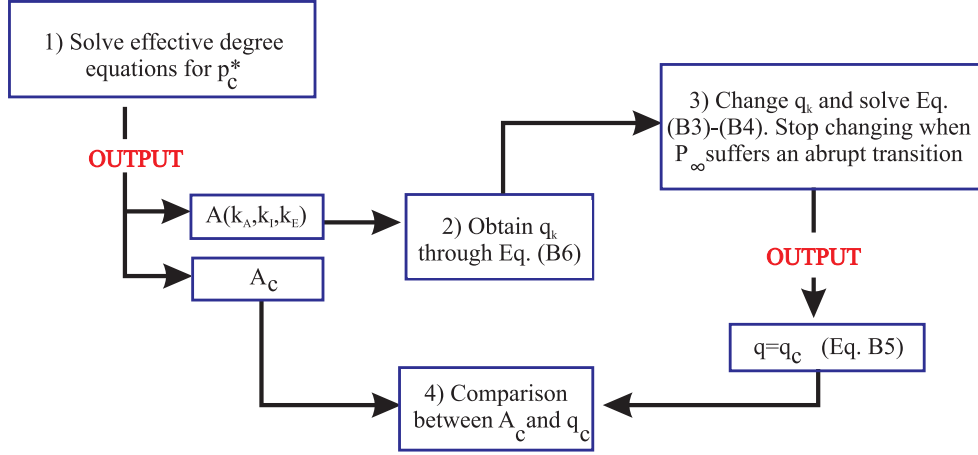


FIG. 14: Flow diagram to compute  $q_c$  in targeted  $k$ -core percolation

### Acknowledgments

We wish to thank to UNMdP, FONCyT and CONICET (Pict 0429/2013, Pict 1407/2014 and PIP 00443/2014) for financial support. We also thank Dr. G. G. Izús and Dr. H. H. Aragão Rêgo for useful discussions.

### Bibliography

- [1] A. E. Hudson, D. P. Calderon, D. W. Pfaff, and A. Proekt, *Proc. Natl. Acad. Sci. USA* **111**, 9283 (2014).
- [2] I. Bose and B. Ghosh, *J. Biosci.* **32**, 991 (2007).
- [3] A. Majdandzic, B. Podobnik, S. V. Buldyrev, D. Y. Kenett, S. Havlin, and H. E. Stanley, *Nat. Phys.* **10**, 34 (2014).
- [4] P. Van Mieghem, F. D. Sahnehz, and C. Scoglio, in *53rd IEEE Conference on Decision and Control* (IEEE, 2014), pp. 6228–6233.
- [5] J. Lindquist, J. Ma, P. van den Driessche, and F. H. Willeboordse, *J. Math. Biol.* **62**, 143 (2011).
- [6] R. M. Anderson, R. M. May, and B. Anderson, *Infectious diseases of humans: dynamics and control*, vol. 28 (Wiley Online Library, 1992).

- [7] R. Pastor-Satorras, C. Castellano, P. Van Mieghem, and A. Vespignani, *Rev. Mod. Phys.* **87**, 925 (2015).
- [8] M. Taylor, P. L. Simon, D. M. Green, T. House, and I. Z. Kiss, *J. Math. Biol.* **64**, 1021 (2011).
- [9] J. C. Miller and I. Z. Kiss, *Math. Model. Nat. Phenom.* **9**, 4 (2014).
- [10] K. Rock, S. Brand, J. Moir, and M. J. Keeling, *Rep. Prog. Phys.* **77**, 026602 (2014).
- [11] J. P. Gleeson, *Phys. Rev. Lett.* **107**, 068701 (2011).
- [12] A. V. Goltsev, F. V. de Abreu, S. Dorogovtsev, and J. F. F. Mendes, *Phys. Rev. E* **81**, 061921 (2010).
- [13] S. N. Dorogovtsev, A. V. Goltsev, and J. F. F. Mendes, *Phys. Rev. Lett.* **96**, 040601 (2006).
- [14] D. Cellai, A. Lawlor, K. A. Dawson, and J. P. Gleeson, *Phys. Rev. Lett.* **107**, 175703 (2011).
- [15] D. Cellai, A. Lawlor, K. A. Dawson, and J. P. Gleeson, *Physical Review E* **87**, 022134 (2013).
- [16] G. Baxter, S. Dorogovtsev, K.-E. Lee, J. Mendes, and A. Goltsev, *Phys. Rev. X* **5**, 031017 (2015).
- [17] M. Molloy and B. Reed, *Random Struct. Alg.* **6**, 161 (1995).
- [18] M. Barthélemy, A. Barrat, R. Pastor-Satorras, and A. Vespignani, *J. Theor. Biol.* **235**, 275 (2005).
- [19] G. Rozhnova and A. Nunes, *Phys. Rev. E* **79**, 041922 (2009).
- [20] G. Rozhnova and A. Nunes, *Eur. Phys. J. B* **74**, 235 (2010).
- [21] M. Kuperman and G. Abramson, *Phys. Rev. Lett.* **86**, 2909 (2001).
- [22] J. C. Miller, A. C. Slim, and E. M. Volz, *J. R. Soc. Interface* **9**, 890 (2012).
- [23] Eigenvalues with a positive (negative) real part corresponds to an unstable (stable) fixed point.
- [24] See classical theorem of Poincaré-Bendixson in Ref. [33].
- [25] P. E. Rapp, *Prog. Neurobiol.* **29**, 261 (1987).
- [26] D. Ghosh, T. Banerjee, and J. Kurths, *Phys. Rev. E* **92**, 052908 (2015).
- [27] J. Lisman and G. Buzsáki, *Schizophr. Bull.* **34**, 974 (2008).
- [28] P. J. Menck, J. Heitzig, J. Kurths, and H. J. Schellnhuber, *Nat. Commun.* **5**, 3969 (2014).
- [29] J. Jalife, R. A. Gray, G. E. Morley, and J. M. Davidenko, *Chaos* **8**, 79 (1998).
- [30] M. San Miguel and R. Toral, in *Instabilities and nonequilibrium structures VI* (Springer,

2000), pp. 35–127.

- [31] A. Majdandzic, L. A. Braunstein, C. Curme, I. Vodenska, S. Levy-Carciente, H. E. Stanley, and S. Havlin, Nat. Commun. **7**, 10850 (2016).
- [32] D. S. Callaway, M. E. J. Newman, S. H. Strogatz, and D. J. Watts, Phys. Rev. Lett. **85**, 5468 (2000).
- [33] F. Verhulst, *Nonlinear differential equations and dynamical systems* (Springer, 2006).